Construction and Building Materials 402 (2023) 132997

Contents lists available at ScienceDirect

Construction and Building Materials

journal homepage: www.elsevier.com/locate/conbuildmat

Experimental and numerical insights on the in-plane behaviour of unreinforced and TRM/SRG retrofitted brick masonry walls by diagonal compression and shear-compression testing

Larisa Garcia-Ramonda [a,*], Luca Pelà [a], Pere Roca [a], Guido Camata [b]

[a] Department of Civil and Environmental Engineering, Universitat Politècnica de Catalunya (UPC-BarcelonaTech), Jordi Girona 1-3, 08034 Barcelona, Spain
[b] Department of Engineering and Geology, University "G. D'Annunzio" of Chieti-Pescara, viale Pindaro 42, I-65127 Pescara, Italy

ARTICLE INFO

Keywords:
In-plane shear behaviour
Tensile strength
Masonry
Textile Reinforced Mortar (TRM)
Steel Reinforced Grout (SRG)
Numerical simulation

ABSTRACT

The experimental determination of the parameters that characterise the in-plane shear behaviour of masonry structures is still a challenging task. Different authors have identified the key role of tensile strength in the definition of the in-plane shear behaviour of masonry, but unfortunately its direct experimental characterisation is not always feasible, and masonry's tensile strength needs to be obtained from complex testing methodologies. As a result, tensile strength needs to be assessed from testing setups such as diagonal compression testing and shear compression testing when the failure mode of masonry is featured by tensile diagonal cracking. However, different formulations are available in the scientific literature regarding the interpretation of the experimental results derived from such tests. This work provides new insights on the interpretation of in-plane shear experimental behaviour of double-leaf historical clay brick masonry walls with low strength mortar joints, both unreinforced and retrofitted with textile reinforced mortar and steel reinforced grout. The research evaluates results derived from both testing methodologies, and investigates the potential correlation between them to fully characterise the in-plane shear behaviour of masonry walls. Finally, a numerical model is used to simulate each testing configuration and study the stress state at the centre of the walls to determine the tensile strength and its correlation with the shear strength and the maximum load attained.

1. Introduction

The experimental evaluation of the in-plane shear strength of unreinforced masonry walls (URM) plays a crucial role in their seismic assessment and hence in the design of possible retrofitting solutions. A direct approach to estimate the shear strength consists of performing experimental tests with proper boundary conditions and acting forces. However, and due to its complex and composite behaviour, masonry may experience different failure modes under lateral loading, depending on the relative mechanical properties of the constituents, the boundary conditions, the wall geometry, and the level of vertical load acting on the structure [1,2]. The three possible failure modes are shear failure due to tensile diagonal cracking, shear failure due to sliding along the bed joints, and rocking failure involving crushing of the compressed corner [3]. Different analytical models [4,5], based on different hypotheses and governing parameters, have been adopted to understand the in-plane shear response of masonry structures and estimate their load capacity. The governing parameters needed for each analytical model are often experimentally determined.

Following different standards and current codes, there are different testing methodologies available to assess the parameters to characterise the in-plane behaviour of masonry. The direct shear tests of masonry couplets or triplets, the diagonal compression test (DCT), and the shear compression test (SCT). The shear strength exhibited by a masonry wall does not only depend on the material properties but also on the boundary conditions featuring the set-up configuration, making it difficult the assessment in an unbiased way. Available standards such as ASTM [6] or RILEM [7], provide guidelines on the masonry specimens, setup configuration, loading protocols and testing conditions for the execution of the DCT.

The direct shear test on small triplets is the simplest and most inexpensive test, but the parameters measured, the cohesion τ_0 and the fiction coefficient μ, are representative of the behaviour of the bed joint rather than of the masonry compound, as stated by Crisafulli, F.J [8]. Therefore, this type of test is useful when the objective is the evaluation of local interaction between constituents (brick and mortar), instead of the assessment of the shear behaviour from a global

* Corresponding author.
E-mail addresses: larisa.garcia.ramonda@upc.edu (L. Garcia-Ramonda), luca.pela@upc.edu (L. Pelà), pere.roca.fabregat@upc.edu (P. Roca), g.camata@unich.it (G. Camata).

https://doi.org/10.1016/j.conbuildmat.2023.132997
Received 28 May 2023; Received in revised form 13 August 2023; Accepted 14 August 2023
Available online 21 August 2023

Nomenclature

α	Coefficient dependent on masonry typology
$\alpha_{\tau,num}$	Coefficient computed from the numerical simulation for τ_{xy}
α_{num}	Coefficient computed from the numerical simulation
μ	Friction coefficient
σ_0	Vertical compression stress
σ_{II}	Minimum principal stress
σ_I	Maximum principal stress
$\sigma_{sl,t}$	Tensile capacity from shear bond test
$\sigma_{u,f}$	Ultimate tensile strength of the textile
σ_x	Horizontal stress
σ_y	Vertical stress
τ_0	Cohesion of mortar joint
τ_{max}	Maximum shear strength
τ_{xy}	Shear stress
$\epsilon_{u,f}$	Strain at failure of the textile
A_n	Cross-section of the wall
b	Geometrical coefficient
E_c	Young's Modulus of masonry
E_f	Young's Modulus of the textile
$f_{b,c}$	Compressive strength of brick
$f_{b,f}$	Flexural tensile strength of brick
f_c	Compressive strength of masonry
$f_{m,c}$	Compressive strength of mortar
$f_{m,f}$	Flexural tensile strength of mortar
$f_{rm,c}$	Compressive strength of mortar matrix
$f_{rm,f}$	Flexural tensile strength of mortar matrix
$f_{t,ASTM}$	Tensile strength according to the ASTM standard
$f_{t,DCT}$	Tensile strength obtained from DCT
$f_{t,SCT}$	Tensile strength obtained from SCT
f_t	Equivalent tensile strength of masonry
$H^{\pm}_{cr,exp}$	Experimental SCT load at cracking
$H^{\pm}_{cr,num}$	Numerical SCT load at cracking
$H^{\pm}_{max,exp}$	Experimental SCT maximum load
$H^{\pm}_{max,num}$	Numerical SCT maximum load
$P_{cr,exp}$	Experimental DCT load at cracking
$P_{cr,num}$	Numerical DCT load at cracking
$P_{max,exp}$	Experimental DCT maximum load
$P_{max,num}$	Numerical DCT maximum load
h	Height of the wall
N	Compressive vertical load during SCT
t	Thickness of the wall
w	Width of the wall

(structural) point of view. The Brazilian test on masonry cores with inclined diametric mortar joint is another approach used for in-situ MDT evaluation [9–11].

Experiments on wall specimens based on DCT and SCT allow the determination of the in-plane shear properties at a structural level. The masonry tensile strength plays a central role in these tests, as highlighted by many authors [4,5,12]. The evaluation of this parameter is possible when the failure of the wall specimens is due to diagonal cracking. There are different theories in the available scientific literature about the interpretation of the experimental results derived from the DCT and SCT, mainly differing in the assumption of the stress state in the centre of the specimen. Since both tests can be used to characterise the parameters that govern the in-plane shear behaviour of masonry, an integrated methodology considering the redundant results derived from both tests allows the achievement of a more reliable characterisation of the in-plane shear behaviour of masonry walls.

Different strengthening techniques have been developed in the last years to improve masonry's in plane shear behaviour. Among these techniques, Textile Reinforced Mortar (TRM) has received much attention due to its mechanical efficiency and its satisfactory compatibility with masonry's substrate. This technique, also denominated Fibre Reinforced Cementitious Matrix (FRCM), consists of externally bonded textiles, such as basalt carbon or glass, embedded into cementitious or lime mortars. A particular case of TRM is the Steel Reinforced Grout (SRG), in which the textile used is typically comprised of ultra high tensile strength steel cords. In spite of its widespread use, the interpretation of the experimental in-plane response of retrofitted masonry is still an open issue.

This work focuses on the interpretation of the results of an experimental campaign involving both testing methodologies, DCT and SCT, on double-leaf masonry walls made of clay bricks and low strength hydraulic lime mortar arranged in Flemish bond, in both the URM and TRM-SRG retrofitted configurations. The research investigates the correlation between the two testing methodologies, from both the experimental and numerical points of view, for the reliable determination of the tensile and shear strength of masonry.

2. Interpretation of in-plane shear tests of masonry walls

2.1. Diagonal compression test (DCT)

The diagonal compression tests is based on loading a masonry assemblage in compression along one of the diagonals, causing a tension failure with the specimen splitting apart in the loading direction. The DCT allows an estimation of the masonry tensile and shear strengths [6,7]. The interpretation of the DCT results is not unique and still raises some uncertainties. In the available standards ASTM and RILEM [6,7], masonry is considered as an isotropic linearly elastic material and its tensile strength f_t is obtained by assuming that the wall fails when the principal tensile stress σ_I attains a maximum value at the centre of the wall. The standards implicitly assume that the stress field inside the panel, when subjected to diagonal compression, is of pure shear and the principal stress directions coincide with the two diagonals of the wall. Therefore, the tensile strength and the shear strength of the wall are the same and can be computed using Eq. (1), where P_{max} is the peak load attained, and A_n is the transversal area of the panel computed according to Eq. (2), in which w, h and t are the width, height and thickness of the wall.

$$f_{t,ASTM} = \tau_{max} = \sigma_I = 0.707\frac{P_{max}}{A_n} \tag{1}$$

$$A_n = t\,\frac{w+h}{2} \tag{2}$$

In 1931 Frocht [13] investigated the stress distribution in a square plate subjected to diagonal compression by means of photoelasticity and analytical derivations. The author demonstrated that, under the hypothesis of an elastic homogeneous isotropic continuum, the stress field was not uniform and the stress state at the centre of the plate was not of pure shear. The author also concluded that normal stress components were present along the horizontal and vertical directions. Eqs. (3) and (4) show the expressions to compute the principal stress proposed by Frocht. Eqs. (5) and (6) express the stress state at the centre of the panel in the global x-y coordinate system.

$$f_{t,Frocht} = \sigma_I = 0.52\frac{P_{max}}{A_n} \tag{3}$$

$$\sigma_{II} = -1.68\frac{P_{max}}{A_n} \tag{4}$$

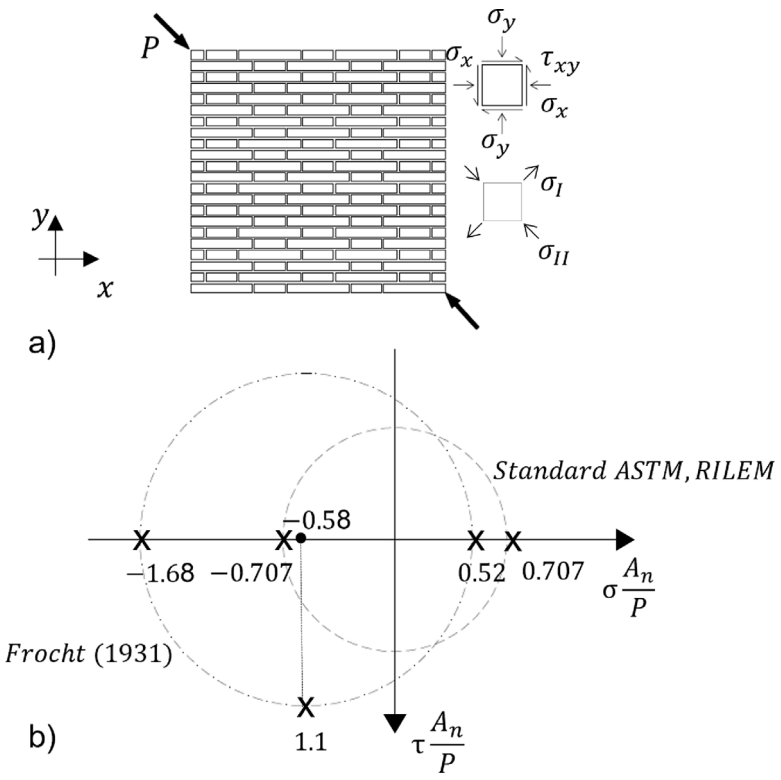

Fig. 1. (a) Stress state in the centre of a wall in DCT as assumed by Frocht [13], (b) Mohr's circle representation according to standards (dashed line), and Frocht's theory (dash-dotted line).

$$\sigma_x = \sigma_y = -0.58\frac{P_{max}}{A_n} \tag{5}$$

$$\tau_{xy} = 1.1\frac{P_{max}}{A_n} \tag{6}$$

Fig. 1-*b* illustrates the corresponding Mohr's circle for both approaches, ASTM/RILEM and Frocht's, according to the stress field defined in Fig. 1-*a*. This figure clearly shows that each approach leads to different estimations of the tensile strength of masonry.

Frocht's interpretation was later validated by Brignola et al. [14]. The author reproduced the problem studied by Frocht with modern numerical methods. The elastic linear solution of an isotropic continuum loaded diagonally, under the hypothesis of plane stress, validated the stress state expressed in Eqs. (3)–(6). In addition, the authors assessed the stress distribution in the non-linear range, which after failure did not significantly influence the value of σ_I. The authors also replaced Eq. (3) with Eq. (7) by introducing a coefficient α dependent on the masonry typology.

$$f_{t,DCT} = \alpha\frac{P_{max}}{A_n} \tag{7}$$

For the case of regular brick masonry, the authors recommended the value of 0.5, which is in line with the findings of Frocht and the recommendation of the Italian building code NTC 2018 [15]. Recent researches [16,17] also validate Brignola et al. findings regarding the definition of the coefficient α for the evaluation of the tensile strength following Eq. (7).

Segura et al. [16] provides a detailed study on the interpretation of the stress state within the masonry panel by means of numerical models accurately calibrated with DCT experimental results. The tests were performed on the same clay brick masonry with low strength mortar that is studied in the present work. The researchers demonstrate that the hypothesis of a pure shear stress state, as defined by the standard [6], is not correct since the normal stresses at the centre of the panel are not null. In a first stage, the research focused on linear analysis, for which the α coefficient was found equal to 0.48, similar to the one proposed by [14] and in agreement with the elastic solutions proposed by [13]. In a second stage of the study, the authors executed a non-linear analysis using a local crack-tracking algorithm and the modified Lubliner damage model proposed by [18], finding an α coefficient equal to 0.40. Finally, the authors observed that the failure of the panel depends on the tensile strength of the material as it triggers the damage. However, the behaviour is complex and there is not a straightforward correlation between the peak load attained and the tensile strength of masonry.

The works carried out by [13,14,16] highlight the need for further research to validate the proposed interpretation of the experimental results to properly estimate the experimental tensile strength of masonry. Such interpretation lays on a twofold premise: first, the stress state at the centre of the panel is not of pure shear, second, for each masonry typology there is a coefficient α that correlates the tensile strength with the peak load experimentally attained P_{max}.

As a result, it emerges the need to define an improved correlation by including additional considerations based on further experimental evidence.

2.2. Shear compression test (SCT)

The SCT test method allows the evaluation of the shear strength as the average shear stress associated to given values of vertical compression and horizontal in-plane loading. The advantage of this test is that the boundary conditions and the loading method induce at the centre of the panel a stress state that closely resembles the one experienced by the wall when subjected to seismic action.

Turnšek and Čačovič [4] proposed a criterion to predict the shear capacity of a masonry wall failing due to tensile diagonal cracking, which was one of the most common failure modes observed in past earthquakes [19,20]. The criterion describes masonry as an equivalent isotropic material and is based on the assumption that failure occurs when the maximum principal stress σ_I at the centre of the wall exceeds

a reference value. Such value is understood as the value of the tensile strength, which represents a characteristic property of masonry. Despite the fact that masonry is far from being an isotropic material, the criterion presents the advantage of characterising the in-plane shear capacity by only one parameter, the tensile strength of masonry f_t. As a result, the shear capacity of the wall, H_{max}, is evaluated following Eq. (8), which was experimentally validated by the authors [4]. In the equation σ_0 is the compressive stress due to the vertical load N, b is a geometrical coefficient that takes into account the distributions of the stresses at the centre of the wall and A_n is the transversal area of the wall.

$$H_{max} = A_n \frac{f_t}{b}\sqrt{1+\frac{\sigma_0}{f_t}} \tag{8}$$

A later research [21] defined the coefficient b as dependent of the shape and geometry of the wall and computed it as the ratio between the dimensions, height h and width w, of the wall ($b = h/w$).

2.3. Correlation between DCT and SCT results

This research contributes to a better understanding of the relationship between the results of the DCT and SCT configurations. As show in the following discussion, only limited references are available in the scientific literature on this topic.

Borri et al. [22] studied the correlation between DCT and SCT for a total number of thirty-five specimens, among which nineteen were manufactured in the laboratory in the unreinforced configuration and sixteen were cut from six existing buildings. In total, fourteen specimens were tested under DCT and the remaining twenty-one were subjected to SCT. The study aimed to validate the two test methods and to discuss and compare the results in terms of shear strength for similar wall panels. The shear strength from DCT, τ_{0D}, was computed according to Eq. (9) and the shear strength from SCT, τ_{0T}, was computed according to Eq. (10), following the Italian building code NTC 2008 [23].

$$\tau_{0D} = \frac{f_{t,D}}{1.5} \qquad f_{t,D} = 0.5\frac{P_{max}}{A_n} \tag{9}$$

$$\tau_{0T} = \frac{f_{t,T}}{1.5} \qquad \tau_{max} = \frac{T_{max}}{A_n} = \frac{f_{t,T}}{b}\sqrt{1+\frac{\sigma_0}{f_{t,T}}} \tag{10}$$

where $f_{t,D}$ and $f_{t,T}$ is the tensile strength of masonry computed for each type of test, P_{max} is the peak load attained from DCT, while T_{max} is the peak shear load attained at SCT, and σ_0 is the vertical compressive stress experienced by the wall during the testing.

From the eight couples of specimens tested with DCT and SCT, the authors defined the ratio $r = \tau_{0T}/\tau_{0D}$, which varied in a range from 1.13 to 3.10 depending on the masonry typology, which included double-leaf rubble stone masonry, and double-leaf and single-leaf solid brick masonry. The results did not evidence a unique correlation of general validity between the shear strength yielded from both test configurations.

Ferretti et al. [24] presented an extensive in-situ experimental campaign on rural masonry, on which minor destructive tests (MDT), and destructive tests, such as DCT and SCT, were conducted. Among the different failure criteria examined (Mohr–Coulomb, Turnšek and Čačovič, and Mann and Müller), the authors found the Mohr–Coulomb's criterion to be the most appropriate to predict the shear behaviour of the masonry under study, which was characterised by its poor quality and was subjected to low compressive stresses.

This work intents to provide new insights on the correlation between the two testing methodologies, DCT and SCT, to characterise effectively the in-plane behaviour of masonry in the URM and TRM/SRG retrofitted configuration. This paper has the triple aim of validating DCT as a simpler standardised test to evaluate the tensile strength of masonry due to diagonal cracking, correlating the experimental response of both testing methodologies to obtain an accurate value of the coefficient α [14], and define an equivalent tensile strength f_t that takes into account the joint action of the masonry wall and the TRM/SRG strengthening system. To fulfil these goals, the DCT and SCT experimental results derived from eight pairs of samples, including unreinforced (URM), repaired and retrofitted with Low Density Basalt fabric (UMR_R), and just retrofitted with Low Density Basalt and Low Density Steel fabrics (LDB and LDS), are analysed and compared. A numerical model was calibrated to accurately simulate both experimental test methodologies, enabling the study of the stress state of the specimens in each testing configuration.

Table 1
Mechanical properties of the materials used for the construction and reinforcement of the walls and of masonry composite.

Brick	$f_{b,c}$ [MPa]	$f_{b,f}$ [MPa]
Average	17.99	2.44
C.O.V	8.30%	20.00%
Mortar	$f_{m,c}$ [MPa]	$f_{m,f}$ [MPa]
Average	2.51	0.66
C.O.V	24.25%	24.00%
Masonry	f_c [MPa]	E_c [MPa]
Average	6.5	2318
C.O.V	9.00%	7.60%
Matrix Mortar	$f_{rm,c}$ [MPa]	$f_{rm,f}$ [MPa]
Average	14.04	4.34
C.O.V	10.50%	17.70%

3. Experimental programme

This section summarises the experiments with DCT and SCT recently carried out at the Laboratory of Technology of Structures and Construction Materials (LATEM) at the Universitat Politècnica de Catalunya (UPC-BarcelonaTech).

3.1. Masonry specimens

Sixteen double-leaf masonry walls, with average dimensions 1270 × 1270 × 310 mm^3, were built using handmade solid clay bricks fired with traditional procedures and hydraulic lime-based mortar. The specimens were built in Flemish bond with 21 courses and 15 mm thick mortar joints as shown in Fig. 2-c. Eight of the specimens were tested under DCT, and the remaining eight under SCT. Each test was carried out on a pair of walls in four different configurations: unreinforced (URM), repaired and retrofitted (URM_R), retrofitted with Basalt Textile Reinforced Mortar (BTRM) and retrofitted with Steel Reinforced Grout (SRG).

The brick's mechanical properties were determined based on compression and flexural tests following the EN 772-1:2011 [25], the EN 772-6:2001 [26]. The mortar used to bind the units was derived from a hydraulic lime-based commercial premix by reducing its compressive strength with limestone filler addition in order to replicate a low strength historical lime mortar according to the procedure proposed in [27]. Following the EN 1015-11:1999 [28], prismatic samples with dimensions 160 × 40 × 40 mm^3 were prepared during the construction of each wall, to evaluate the strength of the mortar. The compressive strength of the masonry was studied in [29]. The value was obtained by means of an extensive experimental campaign involving two different types of standard specimens, the running bond walls and the stack bond prisms. The experimental compressive strength experimentally obtained compared well with the available predictive equations of two different standards, EC6 [30] and ACI [31]. Table 1 summarises the experimental characterisation of each component materials in terms of average values and coefficient of variations (C.o.V).

The damaged specimens URM_R, were first tested in the unreinforced configuration, damaged and later repaired using a combination

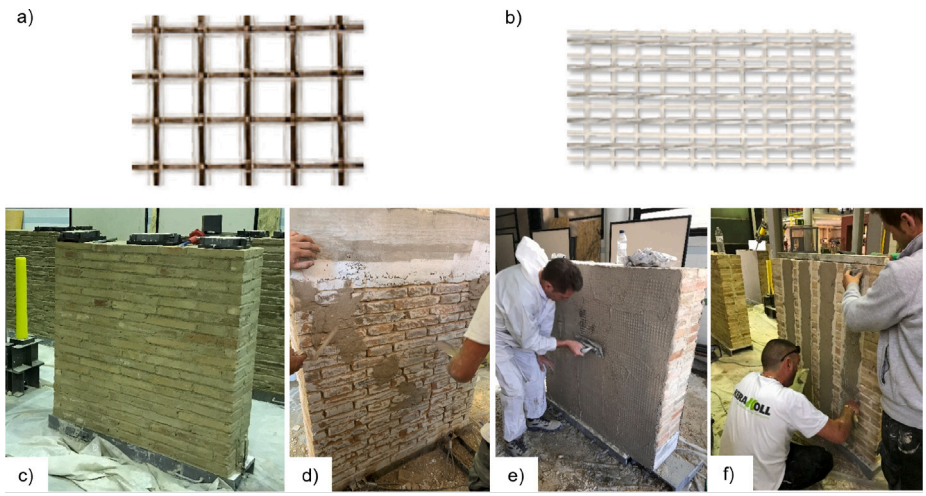

Fig. 2. (a) Bidirectional low density basalt textile (LDB), (b) Unidirectional low density steel textile (LDS), (c) finished look of the masonry specimen in Flemish bond, (d) *scuci-cuci* intervention, (e) strengthening with BTRM, (f) strengthening with SRG.

Table 2
Mechanical properties of the textiles used for the reinforcement of the walls.

	$\sigma_{u,f}$ [MPa]	E_f [MPa]	$\varepsilon_{u,f}$ [MPa]	$\sigma_{sl,t}$ [MPa]
LDB	1700	90	0.019	1049[a]
LDS	2800	190	0.015	2096[b]

[a]for further information [36].
[b]for further information [37–39].

of the *Scuci-cuci* technique and lime mortar repointing, as shown in Fig. 2-*d*. The technique aims at restoring the masonry wall's capacity by substituting the fractured units with new ones of similar properties to ensure a good compatibility. For more information the reader is referred to [32].

For the retrofitting of the masonry walls two solutions were adopted, one involving TRM with bidirectional grid of Low Density Basalt (LDB) textile with a 17 x 17 mm^2 grid spacing, and the other consisting of a SRG solution with one layer of unidirectional ultra-high tensile strength steel cords of low density (LDS) with 1.57 yarn/cm, as shown in Fig. 4-*a,b*. The detailed procedure followed for the implementation of the BTRM (Fig. 4-*e*) and SRG (Fig. 4-*f*) can be found in [32,33], respectively. Table 2 reports the relevant properties of the textiles used for the retrofitting, as provided by the manufacturer and some specific studies, where $\sigma_{u,f}$, E_f and $\varepsilon_{u,f}$ are the ultimate tensile strength, the Young's Modulus and the strain at failure of the textile, respectively. These values are provided by the manufacturer from tensile tests on specimen of 100 mm width as suggested by the American guideline ACI 549.4R-13 [34]. The parameter $\sigma_{sl,t}$ is the tensile strength of the textile when the failure is due to debonding. The term $\sigma_{sl,t}$ is obtained from the single lap shear bond test following the procedure presented in [35].

3.2. DCT experimental set-up

The standard ASTM E519M [6] was used as reference for the execution of the DCT. However, a different setup than that suggested by the aforementioned standard was designed to allow the application of the diagonal compression load without needing the 45 degree rotation of the walls [40]. This modification was needed, due to the low strength binding mortar, in order to avoid the risk of damaging the specimens while rotating them in the laboratory.

The specimens were set on a metallic bench consisting of two parallel H-Shape beams anchored to the strong floor of the laboratory. The metallic profiles, supporting the specimens, were bolted on top of the bench in order to avoid their displacement during the execution of the test. Two steel wedges were placed at two diagonally opposite corners of the specimen. Each wedge was welded to a robust beam consisting of 2 C Channels placed back to back and stiffened with ribs. The beams at each corner were connected with two dywidag bars. The gap between the steel wedges and the corners of the masonry specimens was filled with a layer of epoxy resin and a sheet of compressed wood to smooth the loading surface. The load was applied by using two hydraulic actuators which provided the diagonal force by pulling the dywidag bars, as shown in Fig. 3-*a*. The tests were all performed under displacement control, at a constant displacement rate of approximately 0.5 mm/min.

3.3. SCT experimental set-up

Fig. 3-*b* shows the general view of the experimental set-up for the cyclic shear compression test. During construction, the samples were laid on a metallic C-profile filled with concrete. This base was constrained at both ends by two T-shape devices, in order to prevent the sliding of the specimen along the smooth strong floor of the laboratory when it was subjected to horizontal loading. Both the base and the end-devices were anchored to the strong floor of the laboratory by means of post-tensioned dywidag rebars. On top of the wall a reinforced concrete beam was placed, with the double function of ascertaining the smooth distribution of the vertical load and allocating the plates receiving the horizontal cyclic loading induced by the actuator. On top of the RC beam, a stiff metallic H profile stiffened with ribs was laid, on which the vertical load was applied. Between the RC beam and metallic profile, a 3 mm thick Teflon sheet and a 3 mm thick PVC sheet were inserted to provide a smooth horizontal surface and avoid the shear deformation of the vertical jack caused by the friction generated by the horizontal loading of the wall. Between the RC beam and the PVC sheet a layer of cement-based mortar, with thickness of 5 to 10 mm, was inserted in order to level the end surface of the beam and guarantee the vertical load transfer avoiding stress concentration due to irregularities.

The shear compression tests were performed in two steps. Firstly, the vertical force N was gradually applied under force control. The valves of the jacks were closed once the designed compression stress was reached. Such compression stress was taken equal to $\sigma_v = 0.3$ MPa, which corresponds to a typical vertical load for a two-storey masonry building. Secondly, the imposed horizontal displacement was applied with a hydraulic actuator that enabled the application of cyclic loading in the horizontal direction by means of a hinge. With the valves of the actuators closed, no vertical displacement or rotation of the top of the wall was possible at this stage, and applying horizontal load

Fig. 3. Experimental setup: (a) Diagonal compression test, (b) Cyclic shear compression test.

induced a double bending condition [41]. To control that this boundary condition was enforced, an inclinometer was installed on the top of the metallic beam to measure its rotation during the test. The values recorded by this sensor were in the range of zero degrees showing that no perceptible rotation was experienced by the top of the wall.

The loading protocol of SCT was designed following FEMA 461 [42]. The loading history consisted of repeated cycles of step-wise increasing deformation amplitudes. Three cycles at each displacement amplitude were completed.

4. Correlation between DCT and SCT experimental results

4.1. Experimental results

For the sake of simplicity, only a brief summary of the experimental results is displayed in the following. For a complete analysis of the results from both experimental campaigns, the reader is referred to [40] for DCT and [32,33] for SCT.

Fig. 4-*a* presents the experimental load–displacement curves of all the specimens tested under DCT. All the specimens were characterised by diagonal crack pattern along the compressed diagonal. The cracks started from the centre and propagated progressively towards the corners of the specimen. The URM specimens were characterised by a stair-step diagonal cracking with splitting of units and a sudden drop of strength shortly after the attainment of the peak load. The retrofitted specimens with BTRM and SRG evidenced a post-peak branch characterised by a significant residual resistance, as a consequence of the progressive redistribution of the stresses along the grid and strips of the retrofitting solution. Consequently, the diagonal crack patterns of the retrofitted specimens showed larger areas of damage. Fig. 5-(*up*) displays the characteristic crack patterns of each type of retrofitted configuration tested under DCT.

Fig. 4-*b* shows the experimental force–displacement envelope curves, derived from the experimental hysteric curves. In general, all the specimens tested under SCT mainly failed due to tensile diagonal cracking. Out of the eight specimens tested, only specimens BTRM_2 and SRG_1 showed a mixed failure mechanism combining diagonal tensile cracking and frictional sliding along some bed joints. Fig. 5-(*down*) displays the characteristic crack patterns of each type of retrofitted configuration tested under cyclic SCT.

Table 3 summarises the peak load attained on both testing methodology by each specimen's configuration. In the case of SCT, the parameter H_{max} is the average peak load considering both directions i.e. those of pushing and pulling. In addition, Table 3 includes the vertical load recorded at the attainment of the peak load for every specimen tested under cyclic SCT.

4.2. Validation of Turnšek - Čačovič failure criterion

The specimens experienced tensile diagonal failure, and thus, their in-plane behaviour can be described by Turnšek and Čačovič theory [4]. As aforementioned, this formulation was developed under the hypothesis of masonry as a homogeneous and isotropic material. In order to fit the retrofitted specimens into this criterion, strengthened masonry is hereby considered as a homogenised material, comprising both clay brick masonry and the TRM/SRG strengthening system working together as an equivalent continuum. The assumption seems to be valid since specimens retrofitted with TRM have shown, for both testing methodologies, a homogenising behaviour reducing the scattering between experimental results. Eq. (8) can be used to assess the tensile strength f_t, independently of their configuration -unreinforced or retrofitted- given the experimental lateral capacity of the walls. It must be highlighted that in the cases of retrofitted masonry the parameter f_t represents an equivalent tensile strength that takes into account the joint action of both the masonry wall and the TRM/SRG strengthening system. For the sake of clarity, from now on f_t will be considered as an equivalent tensile strength independently of the specimens' configuration.

To validate the Turnšek and Čačovič criterion [4], the problem presented by Eq. (11) has to be solved. Considering the experimental results from SCT, in particular the values of the peak load H_{max}, the cross section of the specimen A_n and the corresponding level of compression at the attainment of the peak load (N) measured by means of pressure transducer during testing, $f_{t,SCT}$ can be computed for every specimen tested in SCT. The results are included in Table 3.

The yielded values of $f_{t,SCT}$ show a grouping tendency into two experimental groups, i.e. specimens URM and URM_R, and strengthened specimens with TRM/SRG. Fig. 6 shows the H-N interaction diagram in terms of peak loads H_{max} and their corresponding vertical loads N, exhibiting the two aforementioned groups, whose average value of f_t was determined using the least square method to best fit the experimental results of each group of specimens.

$$H_{max} = A_n \frac{f_{t,SCT}}{b} \sqrt{1 + \frac{N}{f_{t,SCT} A_n}} \tag{11}$$

The results are included in Table 3, together with the coefficients of variation (C.o.V) for each group of specimens. This coefficient provides an indication of the level of heterogeneity within each group. The first group exhibits higher scattering than the second, as the URM individual specimens presents inherent heterogeneity of the component materials of URM walls. The lower scattering in the reinforced specimens BTRM

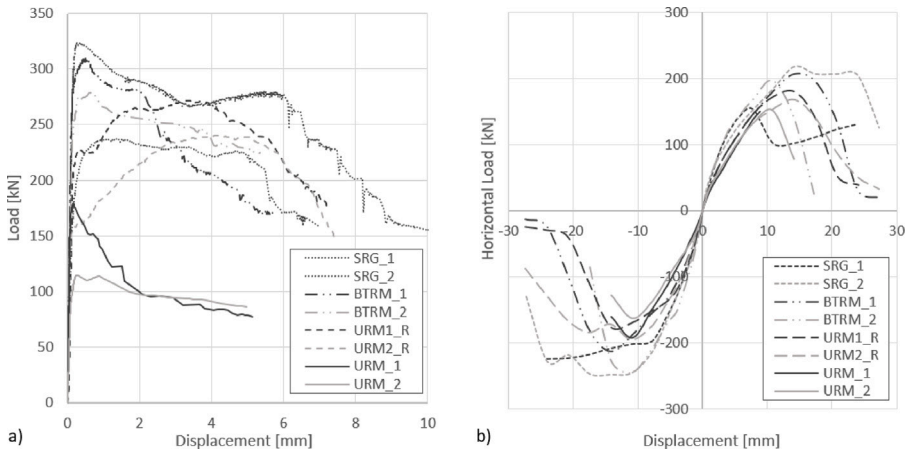

Fig. 4. Experimental results of each specimen tested: (a) DCT: Diagonal compression load–displacement, (b) SCT: Horizontal force–displacement envelope curves.

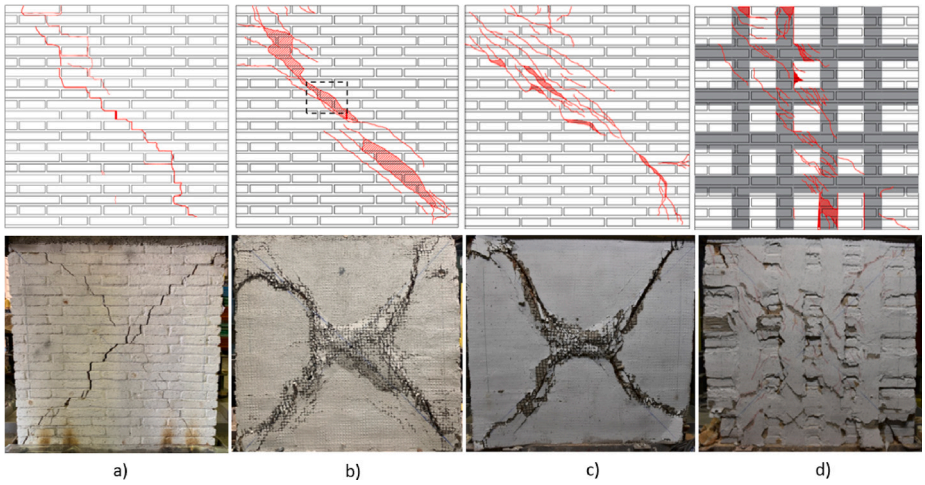

Fig. 5. Characteristic crack pattern of each specimen tested. DCT (*up*), SCT (*down*): (a) URM, (b) URM_R, (c) BTRM, (d) SRG.

Table 3
Experimental results: Peak load recorded for each specimen for each testing methodology, corresponding P_{max} for the peak load from DCT and H_{max} for the peak load from SCT. Vertical load N recorded at the attainment of the peak load during SCT. Equivalent tensile strength yielded from both testing methodologies following Eq. (7) with α equal to 0.40 [16] for computing $f_{t,DCT}$ and Eq. (11) for $f_{t,SCT}$. Computation of the average value of f_t associated to each defined group and its corresponding C.o.V.

Specimen	DCT				SCT				
	P_{max} [kN]	$f_{t,DCT}$ [MPa]	Average [MPa]		H_{max} [kN]	N [kN]	$f_{t,SCT}$ [MPa]	Average [MPa]	
URM_1	184*	0.19	0.19	**0.23** (15.7%)	172	185	0.26	0.24	**0.25** (8.0%)
URM_2					157	203	0.22		
UMR1_R	272	0.26	0.25		178	215	0.26	0.26	
UMR2_R	241	0.24			181	238	0.25		
BTRM_1	310	0.30	0.29	**0.29** (13.6%)	210	247	0.31	0.31	**0.31** (2.9%)
BTRM_2	279	0.27			221	272	0.31		
SRG_1	320	0.33	0.32		224	278	0.32	0.32	
SRG_2	237	0.24			233	293	0.32		

* Average value considering specimens tested in [16] exhibiting the same type of failure.

and SRG can be attributed to the presence of the strengthening system. Consequently, the hypothesis of assuming the strengthened masonry as an equivalent homogeneous isotropic material seems plausible, and the behaviour can be described by Turnšek and Čačovič formulation [4] when the failure is due to diagonal cracking.

As aforementioned in Section 2.1, the interpretation of DCT for defining mechanical properties of masonry, is not univocal.

Table 3 also includes the tensile strength $f_{t,DCT}$ yielded from the experimental results obtained with DCT when applying Eq. (7) and the α coefficient equal to 0.40 obtained in [16]. The values obtained compared fairly well with the ones computed from the experimental results of SCT (Table 3 col. 7).

This result not only validates the DCT as a simpler standardised test to evaluate the equivalent tensile strength of masonry walls from the experimental peak load, but also asserts the use of an α coefficient equal to 0.40 for clay brick masonry walls.

5. Numerical analysis

To validate the experimental interpretation of both testing methodologies, a finite element analysis was executed. This section provides

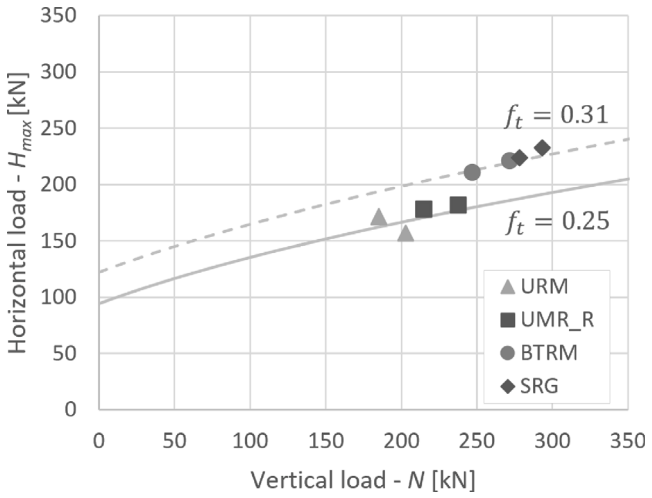

Fig. 6. H-N interaction diagram showing, for all specimens tested, the peak load and corresponding vertical load and its comparison with the ideal curves governed by Eq. (11).

the details of the numerical model employed for the analysis and comparison of the stress states of both experimental setups. The model involved in this analysis was calibrated with the experimental results included in [32,40].

This research focuses on the determination of the tensile and shear strengths of the unreinforced masonry. The homogenisation of the parameters is in line with the hypothesis of homogeneity and isotropy on which the criterion of Turnšek - Čačovič was built upon. At the same time the tensile strength is considered as a global and characteristic parameter of the masonry material.

The computation of the strengths can be latter applied to the design and assessment of retrofitted masonry. As a results, a simple 2D numerical model of the unreinforced masonry wall, based on the macro-modelling approach, was chosen to simulate both testing configurations, DCT and SCT. Therefore, the calibration of the parameters that accurately describe the response of the wall under both tests' boundary conditions and loading profiles was of paramount importance.

The analyses were performed within the OpenSees framework by using the Scientific ToolKit for OpenSees (STKO) pre- and post-processor [43,44].

5.1. Constitutive model

The non-linear behaviour of masonry was modelled using a tension and compression damage model (TC3D) [18]. The strain-based continuum damage model uses two scalar damage variables that allow the distinction between tensile (d^+) and compressive (d^-) damage, which range from 0 (undamaged material) to 1 (fully damaged material). The constitutive law given in Eq. (12) is characterised by an exponential softening law in tension, and a parabolic hardening – exponential softening curve in compression, as shown in Fig. 7, where $\bar{\sigma}^+$; given by Eq. (13).; and $\bar{\sigma}^-$; following Eq. (14); are, respectively, the positive and negative component of the effective elastic stress tensor $\bar{\boldsymbol{\sigma}} = C : \varepsilon$.

$$\bar{\boldsymbol{\sigma}} = (1 - d^+)\bar{\boldsymbol{\sigma}}^+ + (1 - d^-)\bar{\boldsymbol{\sigma}}^- \tag{12}$$

$$\bar{\boldsymbol{\sigma}}^+ = \sum_{i=1}^{3} \langle \bar{\sigma}_i \rangle \boldsymbol{p_i} \otimes \boldsymbol{p_i} \tag{13}$$

$$\bar{\boldsymbol{\sigma}}^- = \bar{\boldsymbol{\sigma}} - \bar{\boldsymbol{\sigma}}^+ \tag{14}$$

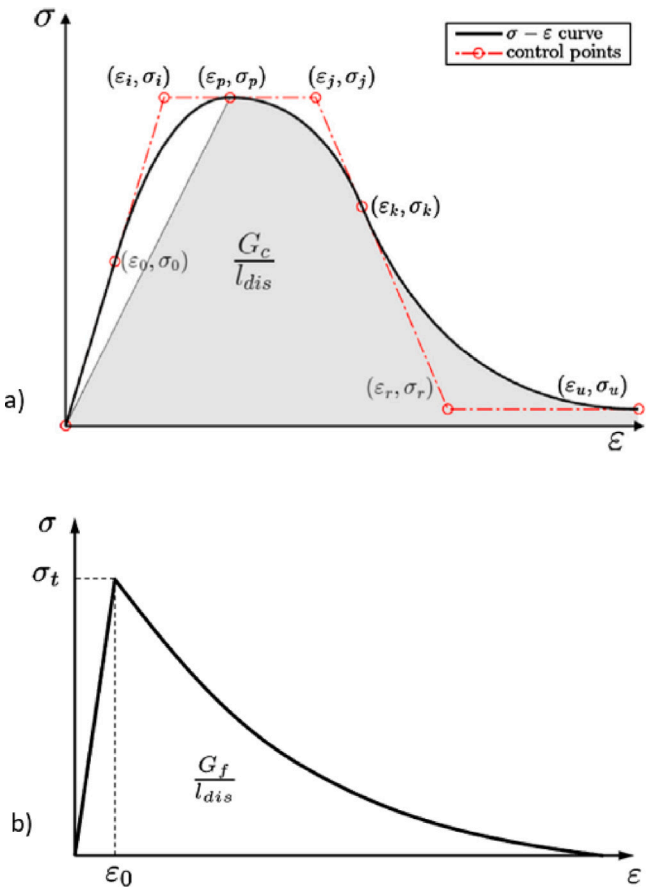

Fig. 7. (a) Compressive uniaxial law, (b) Tensile uniaxial law [18].

Additionally, two scalar measures, τ^+ and τ^-, are introduced to define the shape of the positive and negative damage surfaces, according to Eqs. (15) and (16) respectively.

$$\tau^+ = \frac{1}{1-\alpha}\left(\alpha \bar{I}_1 + \sqrt{3\bar{J}_2} + \beta\langle \bar{\sigma}_{max} \rangle\right)\frac{f_t}{f_c} \tag{15}$$

$$\tau^- = \frac{1}{1-\alpha}\left(\alpha \bar{I}_1 + \sqrt{3\bar{J}_2} + k_1\beta\langle \bar{\sigma}_{max} \rangle\right) \tag{16}$$

$$\alpha = \frac{k_b - 1}{2k_b - 1} \tag{17}$$

$$\beta = \frac{f_c}{f_t}(1-\alpha) - (1+\alpha) \tag{18}$$

where $\bar{I}_1$ is the first invariant of the effective stress tensor, $\bar{J}_2$ is the second invariant of the effective deviatoric stress tensor, $\bar{\sigma}_{max}$ is the maximum effective principal stress, f_c is the compressive stress, f_t is the tensile strength, and k_b is the ratio of the bi-axial strength to the uniaxial strength in compression. The constant k_1 in Eq. (16) enhances the mechanical description of the shear behaviour of the masonry, as it controls the shape of the failure surface in the shear quadrant taking into account the influence that the compressive loading has on the dilatant behaviour of the masonry when subjected to horizontal loading. k_1 ranges from 0 to 1, a value of 0 leads to the Drucker–Prager criterion, while a value of 1 yields a criterion equivalent to the one proposed by Lubliner et al. [45].

The mechanical properties needed to define the model input parameters were: tensile f_t and compressive f_c strengths, tensile G_{ft} and compressive G_{fc} fracture energies, compressive strain at peak ε_p, dilatancy coefficient k_1 and the elastic properties, including the Young's modulus E and the Poisson's ratio ν. The fracture energies G_{ft} and G_{fc},

Table 4
Calibration of the numerical model: input data for the homogenised masonry.

E [MPa]	ν	f_t [MPa]	G_t [N/mm]	f_c [MPa]	G_c [N/mm]	k_1
3450	0.15	0.2	0.01	6.51	9.75	0.16

are defined as energy per unit area. The software STKO for OpenSees, provides an auto-regularisation tool that calculates the specific facture energy according to the characteristic length of the elements used.

5.2. Numerical simulations

The adopted modelling strategy was used to simulate both testing methodologies. For the sake of simplicity, the simulation of the diagonal compression test was performed with an angle of 45 degrees with the load application point on the upper corner of the wall. Unlike the experimental test, the load application was performed through the imposed displacement in the vertical direction with increasing magnitude, while the displacement in the transversal direction was restricted. The diagonally opposite corner was fixed, hindering all displacements.

The simulation of the shear compression test presents the masonry wall confined in between two steel plates. Following the experimental testing procedure, the test was performed in two steps. In the first step, a uniform vertical compression was imposed on the top steel plate. In the second step, the confinement of the wall is achieved by hindering the vertical displacement, and thus, keeping the top of the wall horizontal, as the horizontal load was applied as imposed cyclic horizontal displacement following the same experimental loading protocol defined in [32].

Both tests were analysed under plane stress conditions and displacement control. The discretisation of both specimens consisted of a structured mesh of 2D plane-stress four node quadrilateral elements *(quad)*. Each simulation contained 4608 elements with a mesh size of 20 mm.

5.3. Application of numerical models

In order to numerically investigate the state stress experienced by the URM wall under two distinct testing setups, the adopted model has to be properly calibrated. To this aim, the choice of a suitable reference measurements for the comparison between experimental and numerical curves was crucial.

The homogenised mechanical properties of masonry of the numerical macro-model was calibrated to fit simultaneously the experimental load–strain curves of the DCT and the SCT. Such experimental curves were obtained from the reading of the LDVT sensors placed along the diagonals of the walls on both testing configurations. These magnitudes were compared with the numerical strains calculated between two nodes located on the diagonal of the wall. These four nodes acted as two virtual LVDTs located at an equivalent position to that of the experimental ones. Fig. 8 shows the load–strain curve for the DCT and the envelope curve for the SCT obtained with the numerical simulation, and the comparison with the experimental curves of the LVDT reading of each diagonal on each testing configuration. The experimental strains were computed with the values registered in the LVDTs, divided by their reference length measured before the test and averaged.

The mechanical properties used as the final input for the numerical model for both testing configurations are included in Table 4. The reader is referred to [16] for further details on the calibration of each parameter.

Table 5 presents the comparison between the numerical and experimental output of the URM specimen for both testing configurations. The comparison is mainly focused on the cracking and peak loads, as well as the load–strain behaviour as shown in Fig. 8. The parameter $P_{max,exp}$ is the one corresponding to the specimen URM_1 of the experimental research in [40]. The response of specimen URM_2 was disregarded since its cracking and peak loads were considered unrepresentative of the strength of the URM when compared with a larger data set as provided by [16]. The cracking and peak loads, $H^{\pm}_{cr,exp}$ and $H^{\pm}_{max,exp}$, correspond to the average value attained by both specimen for each direction [32].

The numerical simulations were able to accurately describe the specimens' behaviour in both testing configurations. In most cases, the comparison between experimental and numerical parameters shows a difference always lower than 10%.

6. Analysis of the stress state to validate the tensile and shear strength

The previous section validate the chosen numerical model to satisfactorily simulate the response of URM specimens under DCT and SCT. This section seeks to analyse their corresponding stress state at the centre of the panel and validate the three main premises of this research. First, both testing configurations should derive an equivalent value of the tensile strength as a conventional property of the material. Second, there exists a definition of the coefficient α that correlates the outcome of the DCT, as the maximum load P_{max}, with the tensile strength f_t. Finally, a correlation can be defined numerically between the tensile and shear strengths that can be used to characterise the in-plane shear behaviour of URM and TRM/SRG retrofitted masonry.

In the numerical model of each testing configuration, the tensile strength of the material at the centre of the panel is attained at the moment in which the cracking of the wall starts. Fig. 9 shows, for both testing configurations, at damage initiation the values of parameter d^+ accounting for the degradation of specimen due to tensile damage, and the attained maximum principal stress σ_I contour at the same analysis time step. The cracking initiates at 84%$P_{max,num}$ and 62%$H_{max,num}$ for DCT and SCT, respectively. Those values are in agreement with the experimental ones reported in [32,40] respectively, and it also agrees with the results of the research of Segura et al. [16].

Fig. 10 shows the evolution of the maximum principal stress σ_I and the shear stress τ_{xy}, at the centre of the panel, with increasing loading for both testing configurations' simulation. It is evident, that in spite of SCT simulation presenting a deviation of the stress path, as consequence of its cyclic nature, rather than monotonic like DCT, the value of σ_I at maximum capacity is almost the same. In fact, both simulations attained the same σ_I value when reaching 80% of the maximum load, while showing almost identical post peak response. Similar behaviour is observed in the shear stress, however, in this case the maximum is attained at the same time that the peak load, as expected.

Comparing the average experimental values computed from the SCT results (0.24 MPa) and the input tensile strength in the numerical model (0.20 MPa), there is, on average, a moderate difference of only 16% between the numerical and the experimental results. Nevertheless, this difference can be attributed to the inherent scattering of the masonry mechanical properties among the specimens tested.

With these results of the numerical simulation of DCT it can be performed a back-calculation of the α coefficient with Eq. (19), considering the tensile strength used as input, $f_{t,input}$ and the peak load attained $P_{max,num}$. The coefficient α_{num} takes the value 0.44, similar to the value numerically obtained by [16] and consistent with the range proposed by [14], which varies from 0.35 to 0.56 depending on different masonry typologies.

$$\alpha_{num} = \frac{f_{t,input} A_n}{P_{max,num}} \tag{19}$$

The same analysis can be done for the shear stress τ_{xy} experienced at the centre of the wall. A coefficient $\alpha_{\tau,num}$ can be derived, from Eq. (20), to correlate τ_{xy} with $P_{max,num}$ attained.

$$\alpha_{\tau,num} = \frac{\tau_{xy} A_n}{P_{max,num}} \tag{20}$$

Table 5
Comparison between experimental and numerical cracking and maximum loads.

	$P_{cr,exp}$ [kN]		$P_{cr,num}$ [kN]		ΔP_{cr} [%]		$P_{max,exp}$ [kN]		$P_{max,num}$ [kN]		ΔP_{max} [%]	
DCT	143.3		151.0		5.4%		179.1		178.8		−0.2%	
	$H^{\pm}_{cr,exp}$ [kN]		$H^{\pm}_{cr,num}$ [kN]		ΔH_{cr} [%]		$H^{\pm}_{max,exp}$ [kN]		$H^{\pm}_{max,num}$ [kN]		ΔH_{max} [%]	
SCT	−108.4	109.5	−104.9	103.0	−3.2%	−6.0%	−177.7	151.2	−176.2	166.1	−0.8%	9.9%

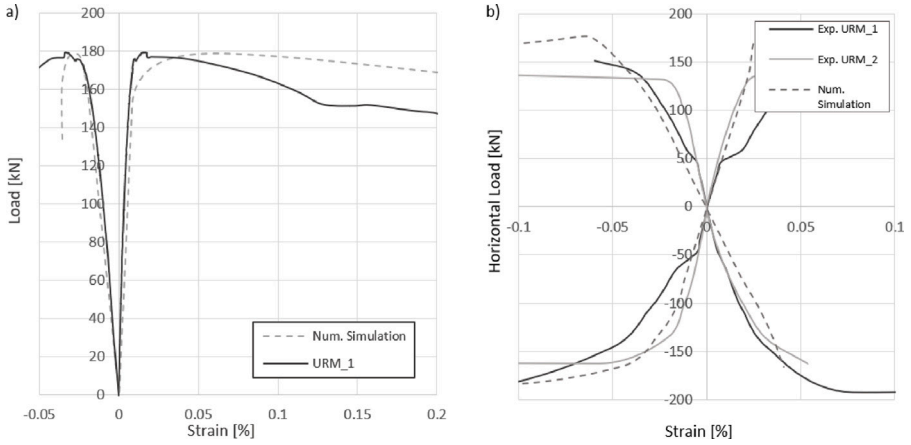

Fig. 8. Comparison between the numerically simulated load–strain curves and the experimental ones: (a) Diagonal compression test, (b) Shear compression test.

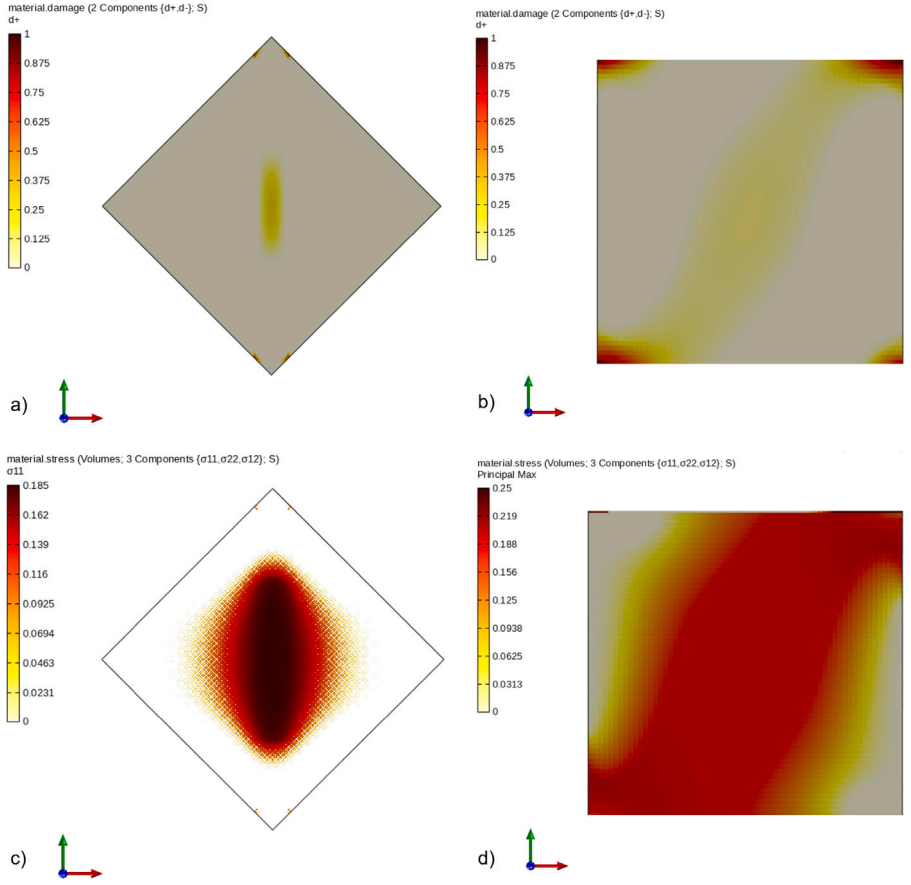

Fig. 9. Tensile damage index d^{+} when cracking starts: (a) DCT, (b) SCT. Contour plot of the maximum principal stress σ_I at the centre of the panel at cracking initiation: (c) DCT, $P_{max,num}$= 151.0 kN (0.84 $P_{max,num}$), (d) SCT, $H_{max,num}$= 103.0 kN (0.62 $H_{max,num}$).

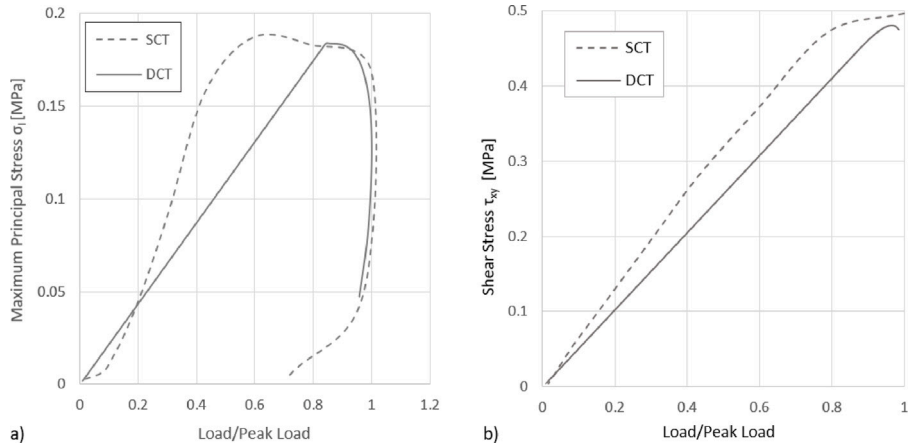

Fig. 10. (a) Evolution of the maximum principal stress σ_I with increasing load at the centre of the wall, (b) Evolution of the shear stress τ_{xy} with increasing load at the centre of the wall. The load is normalised with respect to the maximum load attained during each analysis.

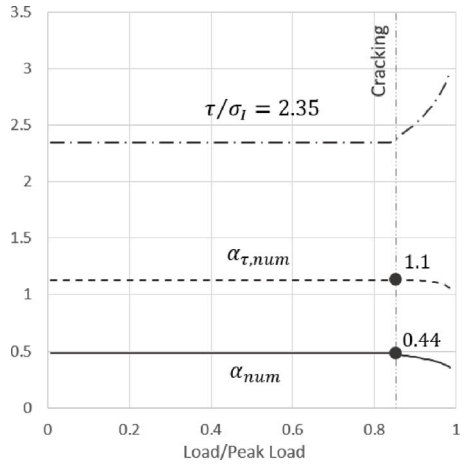

Fig. 11. Evolution of the coefficient α_{num} and $\alpha_{\tau,num}$ with increasing loading. Ratio between the maximum principal stress σ_I and the shear stress τ_{xy}. The cracking point establishes the attainment of σ_I and the coefficient yielded for each case. (The load is normalised with respect to the maximum load attained during each analysis).

Fig. 11 shows the evolution of the coefficients correlating the tensile and the shear stresses with increasing loading from the results of the numerical simulation of DCT. The figure also displays the ratio between the two stresses throughout the test. As previously mentioned, the maximum principal stress is attained at cracking point, which is marked with a double dotted–dashed line in the Figure. After this point the coefficient starts to decrease as a results of the increasing damage. Similar is the behaviour of the coefficient derived for the computation of the shear stress, which interestingly coincides with the one proposed by Frocht [13]. Conversely, the ratio between both stresses spikes after the cracking point, consequence of the different decaying rates of each stress.

Finally, the constant ratio between the stresses, provides a helpful proportionality to properly characterise the in-plane shear behaviour of unreinforced masonry.

7. Conclusion

In the present research a methodology has been derived based on the synergy between two testing methodologies, Diagonal Compression Test (DCT) and Shear Compression Test (SCT), to determine the equivalent tensile strength that describes the in-plane shear behaviour of double-leaf historical clay brick masonry in the unreinforced configuration, failing due to tensile diagonal cracking.

On the main hypothesis of masonry being an equivalent isotropic homogeneous material, the experimental outcome of the URM specimens on both testing configurations were compared to validate a value for the coefficient α equal to 0.40 for the accurate computation of the equivalent tensile strength f_t from the results of the DCT. To validate the applicability of the proposed methodology to the case of strengthened walls, it has been also used to analyse retrofitted masonry specimens with TRM-SRG strengthening systems.

Based on the results obtained from the experimental correlation analysis carried out, the following conclusion can be drawn:

- The same failure mechanism, i.e. tensile diagonal cracking, was experienced by the specimens tested under both testing configurations (DCT and SCT). The failure is accurately described by the simplified model proposed by [4], governed by only one parameter, in this case the equivalent tensile strength f_t, featuring the behaviour of an equivalent isotropic homogeneous material. Therefore, the method discussed in this research cannot be applied to URM structures behaving according to a different failure mode.
- It has been confirmed that the presence of TRM strengthening systems reduces the inherent heterogeneity of the component materials of URM, by reducing the coefficient of variation of the parameters assessed from the experimental outcomes. Consequently, the formulations developed for isotropic homogeneous material such as [4,13], and [14] can be extended to assess the in-plane behaviour of retrofitted masonry.
- The findings validate that both testing configurations yielded the same f_t value. As a result it can be stated that DCT is a simpler standardised test to evaluate the equivalent tensile strength of masonry walls in both configuration, unreinforced and strengthened.
- The comparison of both testing configurations provided an efficient assessment of the value of the coefficient α, as proposed by [14], to correlate the experimental peak load $P_{max,exp}$ and the tensile strength f_t. For the material combination hereby investigated, i.e. double-leaf historical clay brick masonry with low strength mortar joints, a coefficient α equal to 0.40 was validated. Such value differs largely from the one proposed by the current standards ASTM/RILEM for the computation of f_t.

Using a numerical macro model it was also investigated the stress state at the centre of the wall, in both testing configurations. The homogenised masonry properties, were adjusted to fit the experimental curves obtained from both testing configurations.

Based on the results obtained from the numerical correlation analysis carried out, the following conclusion can be drawn:

- The numerical model could be satisfactorily applied to the simulation of the in-plane shear behaviour of the unreinforced masonry wall, characterised by a homogenised material.
- The stress state at the centre of the wall, in both testing configurations, was in correspondence with the findings of Frocht and Segura et al. The simulation exhibited that in the DCT the stress state was not of pure shear, as assumed by the standards, which overestimates the value of f_t and τ_{max}.
- The comparison between DCT and SCT simulations allows the definition of a numerical α_{num} coefficient to correlate f_t with the peak load resulting from the simulation of DCT.

In summary, Eq. (8) can only be applied when dealing with results from SCT, which is an expensive and time-consuming testing methodology. The scientific community is currently arguing when it comes to interpret the results of the DCT to obtain the tensile strength. The main aim of this research was to validate DCT as a simpler and cheaper test to compute the tensile strength of masonry, providing a methodology based on the correlation between the experimental results of DCT and SCT.

Finally, and based on the findings of the present research work, there is a latent need to review and update the coefficient used in the equation of the current standards for the computation of the tensile strength from DCT. In addition, it is of paramount importance to further research on the value of this coefficient for different masonry typologies. Therefore, more experimental tests, combining DCT and SCT in parallel, should be carried out.

CRediT authorship contribution statement

Larisa Garcia-Ramonda: Writing – review & editing, Writing – original draft, Validation, Methodology, Investigation, Formal analysis, Data curation, Conceptualization. **Luca Pelà:** Writing – review & editing, Validation, Supervision, Project administration, Methodology, Investigation, Funding acquisition, Conceptualization. **Pere Roca:** Writing – review & editing, Validation, Supervision, Project administration, Methodology, Investigation, Funding acquisition,Conceptualization. **Guido Camata:** Writing – review & editing, Validation, Software, Methodology, Investigation, Conceptualization.

Declaration of competing interest

The authors declare that they have no known competing financial interests or personal relationships that could have appeared to influence the work reported in this paper.

Data availability

Data will be made available on request.

Acknowledgements

The authors gratefully acknowledge the financial support from the Ministry of Economy and Competitiveness and from the Ministry of Science, Innovation and Universities of the Spanish Government, as well as that of the ERDF (European Regional Development Fund) through the project SEVERUS (Multilevel evaluation of seismic vulnerability and risk mitigation of masonry buildings in resilient historical urban centres, Ref. num. RTI2018-099589-B-I00). The reinforcement systems and construction of the specimens for the experimental programme have been funded by Kerakoll Spa through the RTD project "Seismic Strengthening of Masonry Walls" (Ref. num. A-01278). The authors wish to thank José Luis Sanchez and José Dobón from Kerakoll Spa and Paolo Casadei, for their involvement and support. The support from Agència de Gestió d'Ajuts Universitaris i de Recerca de la Generalitat de Catalunya through a predoctoral grant awarded to the first author is also gratefully acknowledged.

References

[1] A. Preciado, A. Ramirez-Gaytan, Numerical seismic reponse and failure modes of old URM walls under lateral loading, Struct. Anal. Hist. Constr. 18 (2019) 1293–1300, http://dx.doi.org/10.1007/978-3-319-99441-3, URL http://link.springer.com/10.1007/978-3-319-99441-3.

[2] C. Calderini, S. Cattari, S. Lagomarsino, The use of the diagonal compression test to identify the shear mechanical parameters of masonry, Constr. Build. Mater. 24 (2010) 677–685, http://dx.doi.org/10.1016/j.conbuildmat.2009.11.001.

[3] M. Tomaževič, Earthquake-Resistant Design of Masonry Buildings, Vol. 1, Imperial Collage Press, 1999, http://dx.doi.org/10.1142/9781848160835, URL http://ebooks.worldscinet.com/ISBN/9781848160835/9781848160835.html,

[4] V. Turnsek, F. Cacovic, Some experimental results on the strength of brick masonry walls, in: Proc. 2nd International Brick Masonry Conference, 1971.

[5] W. Mann, H. Müller, Failure of shear-stressed masonry - an enlarged theory, tests and application to shear walls, in: Proceedings of the International Symposium on Load Bearing Brickwork, London, 1980, pp. 223–236.

[6] ASTM, Standard test method for diagonal tension (shear) in masonry assemblages, 2000.

[7] RILEM Recommendation for Testing and Use of Construction Material, RILEM TC 76-LUM. Diagonal tensile strength of small wall specimens, E&FN SPON, London, 1994, pp. 488–489.

[8] F.J. Crisafulli, Seismic Behaviour of Reinforced Concrete Structures with Masonry Infills, University of Canterbury, 1997, p. 404, URL http://hdl.handle.net/10092/1221.

[9] D. Marastoni, L. Pelà, A. Benedetti, P. Roca, Combining Brazilian tests on masonry cores and double punch tests for the mechanical characterization of historical mortars, Constr. Build. Mater. 112 (2016) 112–127, http://dx.doi.org/10.1016/j.conbuildmat.2016.02.168.

[10] L. Pelà, P. Roca, A. Benedetti, Mechanical characterization of historical masonry by core drilling and testing of cylindrical samples, Int. J. Archit. Herit. 10 (2016) 360–374, http://dx.doi.org/10.1080/15583058.2015.1077906.

[11] L. Pelà, K. Kasioumi, P. Roca, Experimental evaluation of the shear strength of aerial lime mortar brickwork by standard tests on triplets and non-standard tests on core samples, Eng. Struct. 136 (2017) 441–453, http://dx.doi.org/10.1016/j.engstruct.2017.01.028.

[12] A. Hendry, F. Khalaf, Masonry wall construction, Choice Rev. Online vol. 39 (2001) http://dx.doi.org/10.5860/choice.39-2212.

[13] M. Frocht, Recent advances in photoelasticity and an investigation of the stress distribution in square blocks subjected to diagonal compression, Trans. ASME Appl. Mech. Div. 53 (1931).

[14] A. Brignola, S. Frumento, S. Lagomarsino, S. Podestà, Identification of shear parameters of masonry panels through the in-situ diagonal compression test, Int. J. Archit. Herit. 3 (2008) 52–73, http://dx.doi.org/10.1080/15583050802138634, URL http://www.tandfonline.com/doi/abs/10.1080/15583050802138634.

[15] Ministero delle Infrastrutture e dei Trasporti, DM 17/01/2018 - Aggiornamento delle "Norme Tecniche per le Costruzioni", 2018, pp. 1–198 (in Italian).

[16] J. Segura, L. Pelà, S. Saloustros, P. Roca, Experimental and numerical insight on the diagonal compression test for the shear characterisation of masonry, Constr. Build. Mater. 287 (2021) http://dx.doi.org/10.1016/j.conbuildmat.2021.122964.

[17] F. Ferretti, C. Mazzotti, FRCM/SRG strengthened masonry in diagonal compression: experimental results and analytical approach proposal, Constr. Build. Mater. 283 (2021) http://dx.doi.org/10.1016/j.conbuildmat.2021.122766.

[18] M. Petracca, L. Pelà, R. Rossi, S. Zaghi, G. Camata, E. Spacone, Micro-scale continuous and discrete numerical models for nonlinear analysis of masonry shear walls, Constr. Build. Mater. 149 (2017) 296–314, http://dx.doi.org/10.1016/j.conbuildmat.2017.05.130.

[19] M. Tomaževič, Shear resistance of masonry walls and Eurocode 6 : shear versus tensile strength of masonry, Mater. Struct. (2008) http://dx.doi.org/10.1617/s11527-008-9430-6.

[20] A. Penna, P. Morandi, M. Rota, C.F. Manzini, F.D. Porto, G. Magenes, Performance of masonry buildings during the Emilia 2012 earthquake, Bull. Earthq. Eng. 12 (2014) 2255–2273, http://dx.doi.org/10.1007/s10518-013-9496-6.

[21] V. Turnsek, P. Sheppard, The shear and flexural resistance of masonry walls, in: Proceedings of the International Research Conference on Earthquake Engineering, Skopje, Macedonia [Yugoslavia], 1980, pp. 517–573, http://dx.doi.org/10.1017/CBO9781107415324.004.

[22] A. Borri, G. Castori, M. Corradi, Determination of shear strength of masonry panels through different tests, Int. J. Archit. Herit. 9 (2015) 913–927, http://dx.doi.org/10.1080/15583058.2013.804607.

[23] Ministero delle Infrastrutture e dei Trasporti, Circolare 2 febbraio 2009, n.617. Istruzioni per l'applicazione delle Nuove norme tecniche per le costruzioni, 2009 (in Italian).

[24] F. Ferretti, B. Ferracuti, C. Mazzotti, M. Savoia, Destructive and minor destructive tests on masonry buildings: Experimental results and comparison between shear failure criteria, Constr. Build. Mater. 199 (2019) 12–29, http://dx.doi.org/10.1016/j.conbuildmat.2018.11.246.

[25] CEN, EN 772-1, Methods of test for masonry units. Part 1: Determination of compressive strength, Comité Européen de Normalisation, Brussels, 2011.

[26] CEN, EN 772-6, Methods of test for masonry units. Part 6: Determination of bending tensile strength of aggregate concrete masonry units, Comité Européen de Normalisation, Brussels, 2002.
[27] J. Segura, D. Aponte, L. Pelà, P. Roca, Influence of recycled limestone filler additions on the mechanical behaviour of commercial premixed hydraulic lime based mortars, Constr. Build. Mater. 238 (2020) http://dx.doi.org/10.1016/j.conbuildmat.2019.117722.
[28] CEN, EN 1015-11 - methods of test for mortar for masonry - Part 11: Determination of flexural and compressive strength of hardened mortar, 1999.
[29] J. Segura, L. Pelà, P. Roca, Monotonic and cyclic testing of clay brick and lime mortar masonry in compression, Constr. Build. Mater. 193 (2018) 453–466, http://dx.doi.org/10.1016/j.conbuildmat.2018.10.198.
[30] European Standard, Eurocode 6 - Part 3: Simplified calculation methods for unreinforced masonry structures, 2006.
[31] Building Code Requirements and Specification for Masonry Structures (TMS 402-11/ACI 530-11/ASCE 5-11) Specification for Masonry Structures (TMS 602-11/ACI 530.1-11/ASCE 6-11) and Companion Commentaries Developed by the Masonry Standards Joint Committee (MSJC) Advancing the knowledge of masonry, URL www.masonrysociety.orgwww.concrete.orgwww.seinstitute.org.
[32] L. Garcia-Ramonda, L. Pelà, P. Roca, G. Camata, Cyclic shear-compression testing of brick masonry walls repaired and retrofitted with basalt textile reinforced mortar, Compos. Struct. 283 (2022) http://dx.doi.org/10.1016/j.compstruct.2021.115068.
[33] L. Garcia-Ramonda, L. Pelà, P. Roca, G. Camata, Experimental cyclic behaviour of shear masonry walls reinforced with single and double layered steel reinforced grout, Constr. Build. Mater. 320 (2022) http://dx.doi.org/10.1016/j.conbuildmat.2021.126053.
[34] American Concrete Institute, ACI 549.4r-13 - guide to design and construction of externally bonded fabric-reinforced cementitious matrix (FRCM) systems for repair and strengthening concrete and masonry structures, 2013.
[35] C.N.R. - Consiglio Nazionale delle Ricerche, DT 215/2018 - Istruzioni per la progettazione, l'esecuzione ed il controllo di interventi di consolidamento statico mediante l'utilizzo di compositi fibrorinforzati a matrice inorganica, 2018 (in Italian).
[36] DICAM, Relazione Tecnica sui sistemi di rinforzo Kerakoll applicati a superfici in muratura, Università di Bologna - Scuola di ingegneria e architettura.
[37] S.D. Santis, G. de Felice, Steel reinforced grout systems for the strengthening of masonry structures, Compos. Struct. 134 (2015) 533–548, http://dx.doi.org/10.1016/j.compstruct.2015.08.094.
[38] M. Santandrea, G. Daissè, C. Mazzotti, C. Carloni, An investigation of the debonding mechanism between FRCM composites and a masonry substrate, Key Eng. Mater. 747 (2017) 382–389, http://dx.doi.org/10.4028/www.scientific.net/kem.747.382.
[39] X. Wang, C.C. Lam, V.P. Iu, Bond behaviour of steel-TRM composites for strengthening masonry elements: Experimental testing and numerical modelling, Constr. Build. Mater. 253 (2020) http://dx.doi.org/10.1016/j.conbuildmat.2020.119157.
[40] L. Garcia-Ramonda, L. Pelá, P. Roca, G. Camata, In-plane shear behaviour by diagonal compression testing of brick masonry walls strengthened with basalt and steel textile reinforced mortars, Constr. Build. Mater. 240 (2020) http://dx.doi.org/10.1016/j.conbuildmat.2019.117905.
[41] G. Magenes, G.M. Calvi, Cyclic behaviour of brick masonry walls, in: Balkema (Ed.), Proceedings of the Tenth World Conference on Earthquake Engineering, 19–24 July 1992 Madrid, Spain, 1992, pp. 3517–3522, https://api.semanticscholar.org/CorpusID:204269526.
[42] Applied Technology Council, Interim testing protocols for determining the seismic performance characteristics of structural and nonstructural components - FEMA 461, 2007.
[43] M. Petracca, F. Candeloro, G. Camata, STKO User Manual, ASDEA Software Technology, Pescara, Italy, 2017, p. 227.
[44] M. Petracca, G. Camata, E. Spacone, L. Pelà, Efficient constitutive model for continuous micro-modeling of masonry structures, Int. J. Archit. Herit. 17 (2023) 134–146, http://dx.doi.org/10.1080/15583058.2022.2124133.
[45] J. Lubliner, J. Oliver, S. Oller, E. Oñate, A plastic-damage model for concrete, Int. J. Solids Struct. 26 (3) (1989) 299–326, http://dx.doi.org/10.1016/0020-7683(89)90050-4.